# Prostate deformation from inflatable rectal probe cover and dosimetric effects in prostate seed implant brachytherapy

Jun Lian[a)]
*Department of Radiation Oncology, The University of North Carolina, Chapel Hill, North Carolina 27599*

Yeqin Shao[a)]
*School of Transportation, Nantong University, Jiangsu 226019, China and Department of Radiology and Biomedical Research Imaging Center, The University of North Carolina, Chapel Hill, North Carolina 27599*

Larry D. Potter, Ronald C. Chen, Jordan A. Holmes, and Eleanor A. Pryser
*Department of Radiation Oncology, The University of North Carolina, Chapel Hill, North Carolina 27599*

Jie Shen
*Department of Radiation Oncology, Wenzhou Cancer Hospital/ Wenzhou Central Hospital, Zhejiang 325000, China*

Dinggang Shen[b)]
*Department of Radiology and Biomedical Research Imaging Center, The University of North Carolina, Chapel Hill, North Carolina 27599 and Department of Brain and Cognitive Engineering, Korea University, Seoul 02841, South Korea*

Andrew Z. Wang[b)]
*Department of Radiation Oncology, The University of North Carolina, Chapel Hill, North Carolina 27599*

(Received 6 April 2016; revised 20 October 2016; accepted for publication 27 October 2016; published 17 November 2016)

**Purpose:** Prostate brachytherapy is an important treatment technique for patients with localized prostate cancer. An inflatable rectal ultrasound probe cover is frequently utilized during the procedure to adjust for unfavorable prostate position relative to the implant grid. However, the inflated cover causes prostate deformation, which is not accounted for during dosimetric planning. Most of the therapeutic dose is delivered after the procedure when the prostate and surrounding organs-at-risk are less deformed. The aim of this study is to quantify the potential dosimetry changes between the initial plan (prostate deformed) and the more realistic dosimetry when the prostate is less deformed without the cover.

**Methods:** The authors prospectively collected the ultrasound images of the prostate immediately preceding and just after inflation of the rectal probe cover from thirty-four consecutive patients undergoing real-time planning of I-125 permanent seed implant. Manual segmentations of the deformed and undeformed images from each case were used as the input for model training to generate the initial transformation of a testing patient. During registration, the pixel-to-pixel transformation was further optimized to maximize the mutual information between the transferred deformed image and the undeformed images. The accuracy of image registration was evaluated by comparing the displacement of the urethra and calcification landmarks and by determining the Dice index between the registered and manual prostate contours. After registration, using the optimized transformation, the implanted seeds were mapped from the deformed prostate onto the undeformed prostate. The dose distribution of the undeformed anatomy, calculated using the VariSeed treatment planning system, was then analyzed and compared with that of the deformed prostate.

**Results:** The accuracy of image registration was $1.5 \pm 1.0$ mm when evaluated by the displacement of calcification landmarks, $1.9 \pm 1.1$ mm when characterized by the displacement of the centroid of the urethra, and $0.86 \pm 0.05$ from the determination of the Dice index of prostate contours. The magnitude of dosimetric changes was associated with the degree of prostate deformation. The prostate coverage V100% dropped from $96.6 \pm 1.7\%$ on prostate-deformed plans to $92.6 \pm 3.8\%$ ($p < 0.01$) on undeformed plans, and the rectum V100% decreased from $0.48 \pm 0.39$ to $0.06 \pm 0.14$ cm$^3$ ($p < 0.01$). The dose to the urethra increased, with the V150% increasing from $0.02 \pm 0.06$ to $0.11 \pm 0.10$ cm$^3$ ($p < 0.01$) and D1% changing from $203.5 \pm 22.7$ to $239.5 \pm 25.6$ Gy ($p < 0.01$).

**Conclusions:** Prostate deformation from the inflation of an ultrasound rectal probe cover can significantly alter brachytherapy dosimetry. The authors have developed a deformable image registration method that allows for the characterization of dose with the undeformed anatomy. This may be used to more accurately reflect the dosimetry when the prostate is not deformed by the probe cover.

  

 [http://dx.doi.org/10.1118/1.4967481]

Key words: brachytherapy, ultrasound rectal probe cover, learning based-deformable registration

## NOMENCLATURE

DVH Dose–volume histogram

D100%, D90%, D80% Minimum dose to 100%, 90%, 80% of the structure volume

IntraOp Intraoperative ultrasound image with the inflation from ultrasound rectal probe cover and prostate deformation

PreOp Preoperative ultrasound image with no inflation from ultrasound rectal probe cover and prostate deformation

V150%, V100% Volume of the structure receiving 150% and 100% of the prescribed dose, respectively

## 1. INTRODUCTION

Prostate brachytherapy using permanent seed implant is an important treatment technique for prostate cancer.[1,2] Multiple large studies have established permanent implant brachytherapy as an effective treatment for early-stage disease.[3,4] Toxicity from prostate brachytherapy is correlated with doses to the urethra[5] and rectum.[6] One modern implant technique involves planning, seed loading, and implanting in real time. In this method, prostate ultrasound images are acquired with a transrectal ultrasound probe wrapped in an inflated cover to improve image quality and positioning of the prostate prior to seed implantation.[7] The dose distribution is then optimized within the planning software by adjusting the placement of needles within the prostate volume and the distribution of seeds within each needle. Implantation is guided by superimposing the planned needle position onto the guided ultrasound image, allowing the physician to manipulate the needle until it closely matches the planned location. The ultrasound rectal probe cover remains inflated for the duration of this procedure, resulting in deformation of the prostate volume. Because the dose distribution is optimized using a deformed image of the prostate, differences could potentially exist between the planned dose and the physical dose that is received by the prostate, urethra, and rectum once the probe cover has been deflated. We predict that prostate deformation during the procedure can affect the dosimetry postprocedure without the inflated probe cover.

The goal of this study is to assess the effect of prostate deformation on brachytherapy dosimetry and to develop a novel algorithm that can account for this deformation during brachytherapy planning. Specifically, a learning based deformable image registration algorithm was developed to characterize the voxel-to-voxel correlation between predeformation and postdeformation images of each patient. With this registration, the seed positions within the deformed images were mapped to the undeformed images, allowing for a dosimetric comparison between the clinical plan and the deformation-free research plan.

In this study, the undeformed image refers to the image acquired without inflation of the probe cover. It does not imply that the anatomy was completely free of deformation from alternative causes, like the positions of surrounding organs or the presence of the ultrasound probe itself. The clinical plan refers to the treatment plan designed using the deformed prostate images and delivered to the patient, while the research plan refers to that designed retrospectively using the images of the undeformed prostate.

## 2. METHODS

### 2.A. Patient selection and treatment

This study was approved by the Institutional Review Board of the University of North Carolina. In detail, thirty-four patients with a diagnosis of organ-confined prostate cancer underwent brachytherapy with real-time planning. Selected characteristics of the studied patients are presented in Table I. The clinical procedure follows the standards described by the American Brachytherapy Society for permanent brachytherapy of prostate cancer[8] with intraoperative planning and ultrasound guided needled placement. The details of patients are presented in Table I. Prescribed doses of 145 or 110 Gy were selected for monotherapy or boost treatments, respectively.

The procedure was performed under general anesthesia with the patient in the lithotomy position and a Foley catheter in place. Transrectal ultrasound was used with an inflatable cover wrapped around the ultrasound rectal probe to capture images of the prostate for treatment planning. The preoperative set of ultrasound images were captured preceding probe cover inflation and the contouring was performed after the procedure. The cover was then inflated with sonic conductive gel until the prostate had been raised to the appropriate position with respect to the implant grid. At this point, the intraoperative set of ultrasound images were acquired for treatment planning. The presence of the gel improves acoustic coupling between the soft tissue and the transducer, resulting in an image with superior quality.[7] The prostate, urethra, and rectum were immediately contoured by the physician using

TABLE I. Patient demographic and characteristics.

| | Median (range) |
|---|---|
| Median age | 61 (48–75) |
| Tumor stage | T1c (T1c–T2c) |
| Median Gleason score | 6 (6–7) |
| Mean PSA (ng/ml) | 6.03 (1.2–20.6) |
| Mean prostate volume ($cm^3$) | 34.15 (17.93–72.94) |
| Median number of seeds | 65 (47–105) |
| Median number of needles | 21 (15–31) |

the deformed images. The following dosimetric goals were used while planning: prostate V100% ≥ 95%; D90% between 100% and 115% of prescription dose; urethra V150% ≤ 1 $cm^3$; rectum V100% ≤ 1 $cm^3$.

For treatment planning, the optimization of needles and seeds consisted of three stages. First, a modified peripheral loading method was used to automatically generate a preliminary plan. This method selectively spares the center of the prostate and prioritizes needles placed 5 mm from the outline of the prostate. Second, a dose optimization method was used to strategically adjust source number and distribution to maximally cover the target and spare the organs at risk (OARs) while maintaining the same locations of needles generated by the preliminary plan.[9] Third, the physician manually adjusted the sources and needles to create the final plan. The seeds and spacers were then manually loaded into the needles according to the treatment plan.

Needle placement during the procedure was guided using ultrasound. When the physical location of the needle differed greatly from the planned location, the physician repositioned the needle. Minor differences between the physical and planned needle placements were recorded in the treatment planning software as the procedure took place.[7] This record gives the physician the opportunity to compensate for any deviations between planned and up-to-date dosimetries by shifting the needle position in next implant or supplementing with additional needles. Tracing and real time dose reconstruction were embedded functions in the commercial treatment planning software (VariSeed 8.1).

### 2.B. Equipment

A 3D intraoperative computer planning system (VariSeed ver 8.1; Varian, Inc., Palo Alto, CA) was used for treatment planning and implantation of seeds. Ultrasound images were acquired with a B&K model 1900 biplanar ultrasound machine (B&K Medical, Wilmington, MA). The image resolution was 1 mm in the patient superior–inferior direction and 0.12 mm in the remaining two directions. The ultrasound rectal probe cover was a common type made by CIVCO (Coralville, IA). The probe cover has two layers and an attachment specifically for connecting a syringe to inflate the cover with sonic conductive gel. Loose I-125 seeds (Best Medical International, Springfield, VA and Bard Medical Division, Covington, GA), with an average seed activity of 0.384 ± 0.009 mCi (0.488 ±0.011 U), were used with sterile 18-gauge needles. The seeds were delivered by ultrasound-guided transperineal insertion using the standard 0.5 cm gridded template.

### 2.C. Deformable image registration and seed mapping

In order to map the seeds from the deformed intraoperative (IntraOp) ultrasound images used for the clinical plan onto the undeformed preoperative (PreOp) ultrasound images, a deformable image registration was needed for correlating the voxels between the deformed and undeformed images. Due to the low image contrast and signal to noise ratio, registration between the ultrasound images is a complex problem that has not been thoroughly studied.[10–12]

A hybrid approach was developed in order to map the voxels between the deformed and undeformed prostate. Threefold cross-validation was used in the stage of contour initialization.[13] Patients were randomly assigned to one of the three groups (A, B, and C). The process consisted of three rounds. In each round, two groups were allocated as the training set, with the remaining group used exclusively as the testing set.

The registration part consisted of three steps. First, the contour-to-contour transformations between the binary deformed and undeformed images were found for each patient within the training set. Specifically, the detected centers of the probes in both the deformed and undeformed images were defined as the image origin (0, 0, 0) for each patient, and a cylindrical coordinate system was established along the $z$-axis (superior–inferior direction) for deformed and undeformed images. The best transformation $T'$ was found between the two binary images (contours) using mutual information between the deformed and undeformed images from the same patient. This is described as follows [Eqs. (1) and (2)]:

$$\mathrm{MI}\left(I_{\mathrm{PreOp}},I_{\mathrm{IntraOp}};T\right) = H\left(R_T\left(I_{\mathrm{PreOp}},I_{\mathrm{IntraOp}}\right)\right) + H\left(I_{\mathrm{IntraOp}}\right) - H\left(R_T\left(I_{\mathrm{PreOp}},I_{\mathrm{IntraOp}}\right),I_{\mathrm{IntraOp}}\right) \quad (1)$$

$$T' = \arg\max_{T} \mathrm{MI}\left(I_{\mathrm{PreOp}},I_{\mathrm{IntraOp}};T\right), \quad (2)$$

where $I_{\mathrm{IntraOp}}$ and $I_{\mathrm{PreOp}}$ are the binary deformed and undeformed images from the same patient, $\mathrm{MI}\left(I_{\mathrm{preOp}},I_{\mathrm{intraOp}};T\right)$ is the mutual information of $I_{\mathrm{IntraOp}}$ and $I_{\mathrm{PreOp}}$, $H(I)$ is the Shannon entropy of image $I$,[14] $H(I,J)$ is the joint entropy of images $I$ and $J$, and $R_T(I,J)$ is a registration from $J$ to $I$ with the transformation $T$. Note that the initial value of $T$ is an identity matrix for the binary images and the optimal transformation $T'$ is the best transformation between the binary deformed and undeformed images. Second, the average of the best transformation among patients within the training set was then assigned as the initial coordinate transformation $T_0$ for each patient within the testing set. Last, the deformed and undeformed intensity images were registered on the whole prostate. This was done by detecting the probe centers and establishing the cylindrical coordinate systems for the deformed and undeformed images of patients belonging to the testing group. With the initialization $T_0$, the best transformation $T$ between both the cylindrical coordinate systems of the two intensity images was determined by maximizing the mutual information of the transferred deformed and undeformed images, similar to Eqs. (1) and (2).[15] Despite using only the binary image for registration of the training set, all intensity information was used for registration of the testing set. Please note that during the optimization of this step, $I_{\mathrm{IntraOp}}$ and $I_{\mathrm{PreOp}}$ in Eqs. (1) and (2) are the deformed and undeformed intensity images of the testing patient, $T_0$ is used as the initial transformation, which is derived from the training set, and the optimal transformation $T'$ is the best transformation between the deformed and undeformed images of the current testing patient. Thus, the pixel to pixel correspondence on both the cylindrical coordinate systems was established after an optimal coordinate transformation was found. Using this method, we were able to map the brachytherapy implanted seeds from the deformed prostate onto the undeformed prostate.

It is noted that the initial transformation $T_0$, computed by averaging known transformations, can be applied to a new patient not in training set. The initialization can prevent the registration algorithm from being confined by a local maximum while also reducing the iteration time before convergence. Additionally, the described method can be used on a new patient without the need to segment the undeformed intensity images. The contour of the current patient was not used during the image registration for a given patient. Optimization using Eqs. (1) and (2) parameterized the deformation vector field (DVF) as an modified affine transformation on cylindrical coordinates and regularized by the smoothness of DVF. The transformation is considered linear on the cylindrical coordinate system and nonlinear on the Cartesian coordinate system. A summary of the algorithm is illustrated in Algorithm I of the Appendix. By using the transformation found from the registration, we can transfer the seeds on the intraoperative image to the corresponding preoperative image. With the transferred seeds, brachytherapy dosimetry of the undeformed prostate was calculated using the VariSeed planning software and manual contour on the preoperative image. This plan was then compared to the dosimetry of the clinical plan with the deformed prostate. The inflation of the ultrasound cover was relatively constant along the longitudinal direction and used as an indicator of prostate deformation. The amount of inflation was determined on the axial slice in which the area of the prostate was greatest by measuring the distance between the anterior surface of ultrasound probe and the inflated cover. The workflow of seed mapping and dosimetry comparison is summarized in Fig. 1.

### 2.D. Evaluation of image registration accuracy

Three methods were used to evaluate the accuracy of image registration. The manual contour on the IntraOp image was transferred back to the PreOp image using the transformation found from deformable image registration. The Dice index was calculated using the transferred contour and original manual contour on each PreOp image to evaluate the performance of our image registration method. This serves as a preliminary quality assurance of registration. To further check the pixel to pixel correspondence inside the contour, the calcification points were identified and used as landmarks. The calcifications have been found to be the reliable markers of prostate positioning in cone beam CT guided radiotherapy[16] and quantify the accuracy of image registration.[17] Among 34 patients, 32 patients had visible calcifications. The average number of calcification points of these 32 patients was $1.8 \pm 1.1$ (1–4) per patient. Overall 57 calcifications were used in this evaluation. The calcifications were contoured as small structures in both the IntraOP and PreOp images. After the IntraOp image was registered on the PreOp image, the calcification contour from the IntraOp image was transferred to the PreOp image. The displacement between two calcification landmarks was measured as the distance of the centroids of two contours. Last, the urethra was used to evaluate the accuracy of image registration due to its relatively stable position in the prostate. The urethra was contoured ~3–5 slices (slice thickness is 1 mm) superior and inferior to the prostate contour, dependent on the visibility of the structure. Next we intersected the urethra and prostate. This intersected contour was used later for determining the center of mass, which eliminated the effect of uncertainty from the urethra contours superior and inferior to the prostate. The distance of the centroids of intersected urethra on the transformed IntraOP and original PreOp images was measured.

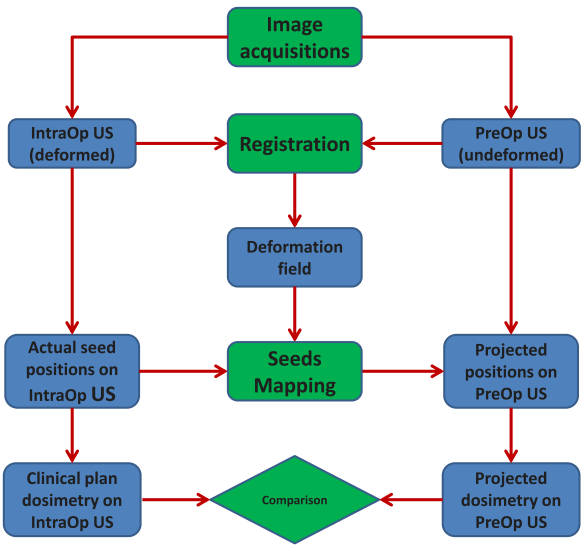


FIG. 1. The workflow of seed mapping and dosimetry comparison.

### 2.E. Statistical testing

The change of dosimetric endpoints was tested with a two-tailed Wilcoxon signed-rank test or Wilcoxon rank-sum test. The significance level was defined as $p = 0.05$. The Pearson correlation coefficient $r$ was calculated to quantify the linear relationship between the change of dosimetry and the inflation of probe cover, which is related to the degree of prostate deformation. All statistical analysis was performed using the MATLAB Statistics Toolbox version 2014b (Natick, MA).

## 3. RESULTS

### 3.A. Prostate deformation and image registration

Qualitatively, there was a significant prostate deformation from the inflation of the ultrasound rectal probe cover. Figure 2 demonstrates the difference in prostate shape before (a) and after (b) cover inflation with the calcification marked. With the established correspondence by the aforementioned deformable image registration, contour and seed locations on the IntraOp (deformed) image could be transferred to the PreOp (undeformed) image. The displacement of all calcification landmarks between two registered images was $1.5 \pm 1.0$ mm on average ($n = 57$; 32 out of 34 patients). The signed displacements in the $x$ (patient left–right), $y$ (patient anterior–posterior), and $z$ (patient superior–inferior)

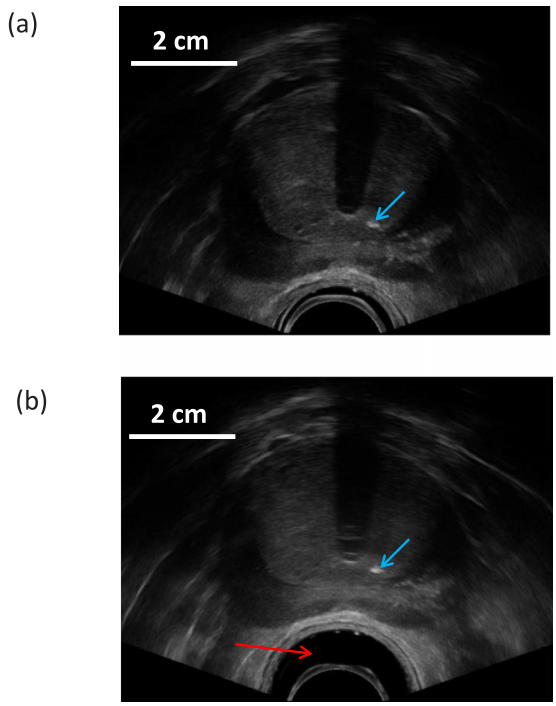


FIG. 2. Prostate deformation resulting from the inflation of the ultrasound rectal probe cover during the seeds implant. (a) PreOp image when the cover is not inflated. (b) IntraOp image when the cover is inflated to elevate the prostate. Red arrow points to the inflated area by probe cover. Light blue arrows point to a calcification in both images. (See color online version.)

directions were $-0.01 \pm 0.10$, $0.07 \pm 0.17$, and $0.83 \pm 1.64$ mm, respectively. The higher average displacement of calcification landmarks in the patient superior–inferior direction was caused by the bigger pixel size in this direction (1 vs 0.12 mm in the other two directions). The displacement of the centroid of the urethra contour inside the prostate was $1.9 \pm 1.1$ mm ($n = 34$). The Dice index between the transferred contour and the original contour was $0.86 \pm 0.05$ ($n = 34$). These indicate that the image registration and transformation of seed positions are relatively accurate.

### 3.B. Dosimetric change between PreOp and IntraOp images

A clinical treatment plan was generated from the IntraOp image [Fig. 3(a)]. The contour, isodose line, and seed positions are displayed on one transverse slice of a sample patient. The seed locations were optimized based on the contours of the prostate and normal structures. When this IntraOp image was registered with the PreOp image using the deformable registration algorithm, the seeds on the clinical plan were also mapped onto the PreOp image. After the seeds on the PreOp image were identified in VariSeed software, the dose distribution was calculated [Fig. 3(b)]. Compared with the dose distribution on the PreOp image [Fig. 3(a)], the 100% isodose line, shown as the green isoline, shifted anteriorly and the 150% isodose line, shown as the yellow isoline, moved closer to the urethra. The overall change of 3D dosimetry of this sample patient is demonstrated in the DVH in Fig. 3(c). A slight reduction of the prostate coverage was evident, from a V100% of 96.4% on

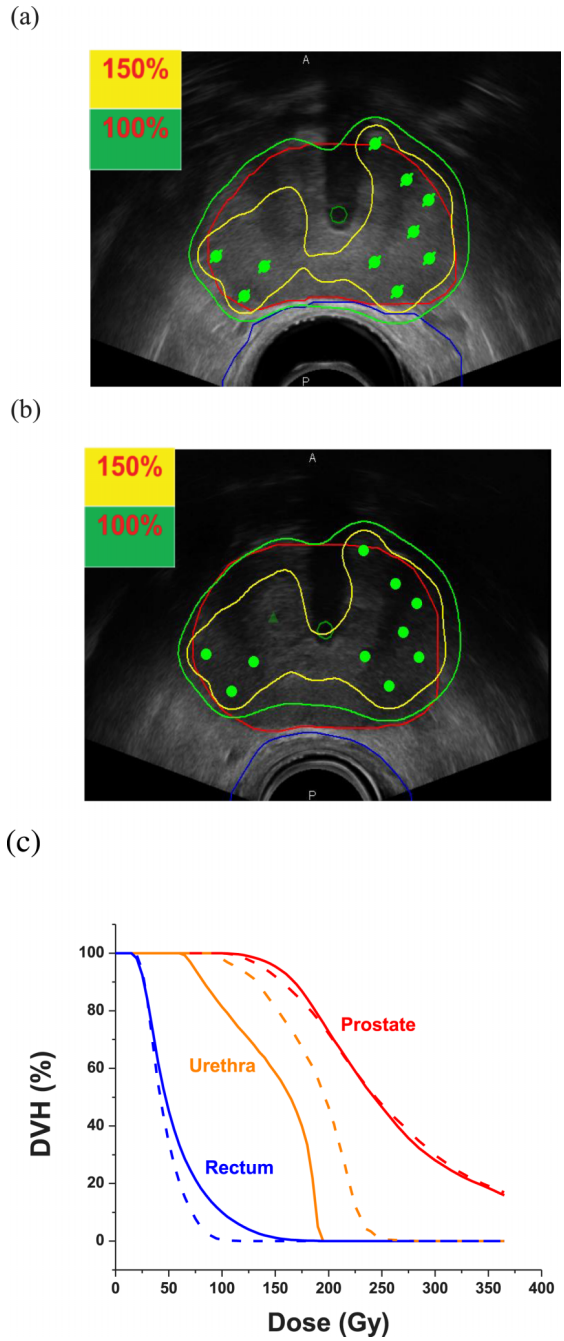


FIG. 3. Prostate seeds mapped from the deformed image to undeformed image and associated dosimetry for a representative patient. (a) Seeds and isodose curves on the clinical plan based on the IntraOp ultrasound image. Red contour is the prostate, blue contour is the rectum, and green circle is the urethra. Solid green circle with cross represents the implanted seed in VariSeed software. (b) Dosimetry based on the undeformed PreOp ultrasound image using seed positions mapped from the deformable registration. Solid green circle is the seed to be implanted and a green triangle points to a seed in a neighboring slice. (c) DVHs of sample clinical plan based on the IntraOp image (solid line; prostate deformed) and research plan based on the PreOp image (dashed line; prostate undeformed). (See color online version.)

the IntraOp image to 93.4% on the PreOp image. Rectal dose was found to decrease as well, from a V100% of 0.49 $cm^3$ on the IntraOp image to 0 $cm^3$ on the PreOp image. The urethra DVH shifted right for this patient, with the D1% increased from 192.0 to 250.3 Gy.

TABLE II. Comparison of dosimetry for the prostate, rectum, and urethra in deformed vs undeformed anatomy.

| | Deformed anatomy | Undeformed anatomy | *P* |
|---|---|---|---|
| Prostate V100% | 95.6% ± 1.7% | 92.6% ± 3.8% | <0.01 |
| Prostate D90% | 113.8% ± 4.0% | 107.4% ± 9.8% | <0.01 |
| Rectum V100% | 0.48 ± 0.39 $cm^3$ | 0.06 ± 0.14 $cm^3$ | <0.01 |
| Urethra V150% | 0.02 ± 0.06 $cm^3$ | 0.11 ± 0.10 $cm^3$ | <0.01 |
| Urethra D1% | 203.5 ± 22.7 Gy | 239.5 ± 25.6 Gy | <0.01 |

The statistical data of all patients ($n = 34$) are summarized in Table II. The coverage of the prostate dropped from 95.6% ± 1.7% in the clinical plans to 92.6% ± 3.8% in the research plans ($p < 0.01$). The D90% showed a similar trend, changing from 113.8% ± 4.0% to 107.4% ± 9.8% ($p < 0.01$). Qualitatively, the drop in dose coverage occurred more at the posterior side of the prostate next to the rectum. As shown in Fig. 3(b), the posterior seeds are shifted more in the anterior direction than the anterior seeds. This agrees with our observation of calcification landmarks. The prostate volume did not show significant differences ($p > 0.05$) between the PreOp image (33.9 ± 10.9 $cm^3$) and the IntraOp image (34.2 ± 11.1 $cm^3$). The rectum showed better sparing in the research plans, with the V100% decreased from 0.48 ± 0.39 to 0.06 ± 0.14 $cm^3$ ($p < 0.01$). However, the urethra received a higher dose in the research plans, with the V150% increasing from 0.02 ± 0.06 to 0.11 ± 0.10 $cm^3$ ($p < 0.01$) and D1% increasing from 203.5 ± 22.7 to 239.5 ± 25.6 Gy ($p < 0.01$).

Inflation of the ultrasound probe cover was measured for all patients and plotted with the change of prostate V100%, rectum V100%, and urethra D1% from the clinical plan to research plan (Fig. 4). The Pearson's correlation coefficients ($r$) were −0.30, −0.37, and 0.04 when a linear regression was made between the changes of prostate V100%, rectum V100%, and urethra D1% and inflation of the probe cover, respectively. This suggests a weak correlation between the displacement and the change of prostate V100% and rectum V100%. The median value of inflation was 6.8 mm. Patients were distributed into two groups, one with relatively small inflation ($d < 6.8$ mm; $n = 17$) and the other with relatively large inflation ($d \geq 6.8$ mm; $n = 17$). The rectum V100% shows a significant difference between the two groups as indicated in Table III.

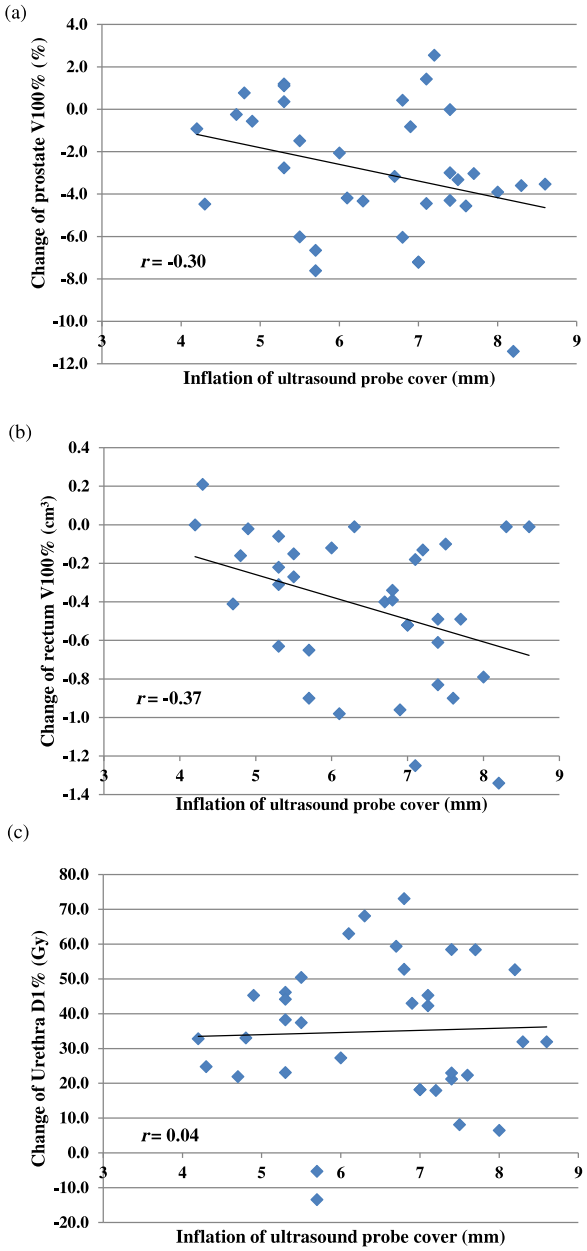


FIG. 4. Change of dosimetric endpoints from the deformed image (clinical plan) to the undeformed image (research plan). (a) Prostate V100%. (b) Rectum V100%. (c) Urethra D1%.

## 4. DISCUSSION

There has been a large body of literature demonstrating the importance of prostate seed implant dosimetry. Correlation has been discovered between poor implant quality and high failure rates.[18] Many studies have also reported that D90% and V100% of the prostate are correlated with treatment outcome.[19–21] Similarly, it is recommended that the critical organ dose parameters, such as the urethra V150, urethra maximum dose (or D1%), and rectum V100%, are to be limited to reduce the side effects.[22] Thus it is very useful to know the accurate dosimetric parameters without the temporary large organ deformation during the procedure.

To our knowledge, this is the first study to examine the impact of the inflated ultrasound rectal probe cover on the dosimetric characteristics in prostate brachytherapy. Adjusting for tissue deformation has been an important topic in the field of radiation therapy. Deformable image registration has been used for structure/target delineation, dose accumulation, and to facilitate adaptive radiation therapy.[23–25] While a number of deformable registration methods have been developed for computed tomography (CT) images,[26] there is a general lack of established methods for ultrasound images and learning-based methods.[10–12] Thus, our study is novel for developing such a method and using it for a clinical study. Our registration method is intensity-based. Unlike feature-based registration methods, our method does not need to compute the

TABLE III. Changes in dosimetric endpoints from the deformed image to the undeformed image caused by the inflation of ultrasound probe cover.

| | Small inflation ($d < 6.8$ mm) | Large inflation ($d \geq 6.8$ mm) | $P$ |
|---|---|---|---|
| Prostate V100% | −2.4% ± 2.7% | −3.4% ± 3.3% | 0.19 |
| Rectum V100% | −0.30 ± 0.32 $cm^3$ | −0.55 ± 0.39 $cm^3$ | 0.04 |
| Urethra D1% | 35.0 ± 21.0 Gy | 34.7 ± 18.7 Gy | 0.72 |

features within the images prior to registration. Additionally, our method employs mutual information as the similarity metric, so it is insensitive to intensity shift between image acquisitions. On the other hand, our method only uses the conventional mutual information and does not consider the spatial information of the image to facilitate registration. The evaluation of registration accuracy involved calcification points. In some patient, there is no clear calcification or the calcification is quite large. More reliable landmarks such as gold fiducials will be used in future efforts to further verify the accuracy of image registration. The registration uncertainty of 1.5 mm found in this study, primarily in the superior-inferior direction, could partially contribute to the reported change in dosimetry; however, we do not believe that it is the main factor.

Through deformable image registration and subsequent dosimetric analysis, we found on the less deformed image that the coverage of the prostate decreased, the rectum was less irradiated, and the urethra received higher dose. The clinical implication of this work is that during a real-time prostate brachytherapy procedure, treatment planning may need to consider the magnitude of prostate deformation from the ultrasound rectal probe cover. Our results show that physicians and physicists may be compromising prostate coverage when attempting to meet the rectal dose constraint during planning. This result is only based on ultrasound images acquired prior to the seed implant during the procedure without the inflation of probe cover. As part of our standard clinical practice, each patient underwent postimplant CT one month postbrachytherapy. Dosimetry is verified based on the CT information. While this is clinically meaningful (avoiding gross over/under dosing of interested structures), it is less sensitive to detect the kind of difference we are investigating in this study. It is known that the volume of prostate on pretreatment ultrasound image and post-treatment CT can be 20% different.[27] This is largely due to the fact that CT imaging does not delineate the prostate accurately (overestimates). There are notable difficulties distinguishing the prostate from other tissues on CT images, especially with the artifacts caused by the implanted metal seeds. Therefore, while we agree that it would strengthen our work with CT dosimetry post-treatment, we do not feel that it is necessary to include in this study. We are devising plans to conduct such a study with more accurate prostate delineation, possibly utilizing MR imaging. In addition, the accumulated dosimetry, especially dose on normal structures, may need more frequent imaging after the procedure to capture the average state of organs. Dosimetry reported in this study was derived on less deformed ultrasound images, instead of more deformed planning image. Therefore, it should be closer to accumulated ideal dosimetry than original planning dosimetry.

Reports on early series of men who underwent a postimplant CT scan for dosimetry purposes showed that cases with a D90 value above a cut point had significantly better prostate-specific antigen (PSA) control than cases below the cut point. This implied that there was a dose–response relationship for local control of the cancer within the prostate.[21,28,29] Zelefsky and Whitmore reported the assessment of the 15-year outcome of the historical series of retropubic freehand implants performed at the Memorial Sloan-Kettering Cancer Center and found that the technique was associated with a greater than expected incidence of local relapse at 15 years. They identified suboptimal dose distribution due to the technical limitations as the possible cause of the unfavorable outcome.[30] The improvement of dosimetry from our method is most likely incremental and may not change the long term disease control for the overall patient population, but for certain patients with large deformation of the prostate during the implant, the dosimetric change may be large enough to cause a difference of treatment outcome. This warrants further long-term investigation to quantify how deformation affects dosimetry and local control.

## 5. CONCLUSIONS

In conclusion, we developed a deformable image registration method that allows a dosimetric estimation using the images of the undeformed prostate. Our study demonstrates that the deformation caused by the inflated probe cover significantly affects the real dose to the target and normal organs in prostate brachytherapy. Our data suggest that treatment planning using images of the deformed prostate can overestimate coverage of the target, rectal dose, and sparing of the urethra. Our method of deformable mapping can be integrated into existing clinical treatment planning tools to account for prostate deformation and report more accurate dosimetry.

## ACKNOWLEDGMENT

Yeqin Shao was supported in part by the National Natural Science Foundation of China (NSFC) under Grant No. 61671255.

## APPENDIX: ALGORITHM OF IMAGE REGISTRATION

Here $T_0$ is the average of transformations between deformed and undeformed images from other patients in the training set based on the cylindrical coordinate system.

ALGORITHM I. Deformable registration between the deformed and undeformed images of the same patient.

**Step. 1.** Detect the centers of the probes in both deformed and undeformed images at the central slice as the original.

**Step. 2.** Establish cylindrical coordinate systems for deformed and undeformed images with the $z$-axis (patient superior–inferior direction).

**Step. 3.** Set transformation $T$ as the initialization $T_0$.

**Step. 4.** Transfer $I_{\text{IntraOp}}$ to $I_{\text{PreOp}}$ of a same patient in the testing set by the deformable transformation $T$.

**Step. 5.** Compute mutual information between $I_{\text{PreOp}}$ and $I'_{\text{IntraOp}}$ (transferred $I_{\text{IntraOp}}$) as a similarity criterion.

$$\text{MI}(I_{\text{PreOp}}, I'_{\text{IntraOp}}) = H(I_{\text{PreOp}}) + H(I'_{\text{IntraOp}}) - H(I_{\text{PreOp}}, I'_{\text{IntraOp}})$$

**Step. 6.** If the mutual information does not converge, set $T = T + \Delta T$, and go to Step. 4, otherwise stop.

**Step. 7.** Obtain the optimal transformation.

[a]Co-first authors: jun_lian@med.unc.edu and hnsyk@163.com
[b]Authors to whom correspondence should be addressed. Electronic addresses: dgshen@med.unc.edu and andrew_wang@med.unc.edu

[1]M. J. Zelefsky, T. Hollister, A. Raben, S. Matthews, and K. E. Wallner, "Five-year biochemical outcome and toxicity with transperineal CT-planned permanent I-125 prostate implantation for patients with localized prostate cancer," Int. J. Radiat. Oncol., Biol., Phys. **47**, 1261–1266 (2000).
[2]P. D. Grimm, J. C. Blasko, J. E. Sylvester, R. M. Meier, and W. Cavanagh, "10-year biochemical (prostate-specific antigen) control of prostate cancer with 125I brachytherapy," Int. J. Radiat. Oncol., Biol., Phys. **51**, 31–40 (2001).
[3]W. J. Morris, M. Keyes, D. Palma, I. Spadinger, M. R. McKenzie, A. Agranovich, T. Pickles, M. Liu, W. Kwan, J. Wu, E. Berthelet, and H. Pai, "Population-based study of biochemical and survival outcomes after permanent 125I brachytherapy for low- and intermediate-risk prostate cancer," Urology **73**, 860–865 (2009).
[4]E. Y. Shapiro, S. Rais-Bahrami, C. Morgenstern, B. Napolitano, L. Richstone, and L. Potters, "Long-term outcomes in younger men following permanent prostate brachytherapy," J. Urol. **181**, 1665–1671 (2009).
[5]T. Zilli, D. Taussky, D. Donath, H. P. Le, R. X. Larouche, D. Beliveau-Nadeau, Y. Hervieux, and G. Delouya, "Urethra-sparing, intraoperative, real-time planned, permanent-seed prostate brachytherapy: Toxicity analysis," Int. J. Radiat. Oncol., Biol., Phys. **81**, e377–e383 (2011).
[6]A. U. Kishan and P. A. Kupelian, "Late rectal toxicity after low-dose-rate brachytherapy: Incidence, predictors, and management of side effects," Brachytherapy **14**, 148–159 (2015).
[7]Y. Yu, L. L. Anderson, Z. Li, D. E. Mellenberg, R. Nath, M. C. Schell, F. M. Waterman, A. Wu, and J. C. Blasko, "Permanent prostate seed implant brachytherapy: Report of the American Association of Physicists in Medicine Task Group No. 64," Med. Phys. **26**, 2054–2076 (1999).
[8]S. Nag, D. Beyer, J. Friedland, P. Grimm, and R. Nath, "American Brachytherapy Society (ABS) recommendations for transperineal permanent brachytherapy of prostate cancer," Int. J. Radiat. Oncol., Biol., Phys. **44**, 789–799 (1999).
[9]Y. Yu, J. B. Zhang, R. A. Brasacchio, P. G. Okunieff, D. J. Rubens, J. G. Strang, A. Soni, and E. M. Messing, "Automated treatment planning engine for prostate seed implant brachytherapy," Int. J. Radiat. Oncol., Biol., Phys. **43**, 647–652 (1999).
[10]D. V. Amin, T. Kanade, A. M. DiGioia III, and B. Jaramaz, "Ultrasound registration of the bone surface for surgical navigation," Comput. Aided Surg. **8**, 1–16 (2003).
[11]J. F. Krucker, G. L. LeCarpentier, J. B. Fowlkes, and P. L. Carson, "Rapid elastic image registration for 3-D ultrasound," IEEE Trans. Med. Imaging **21**, 1384–1394 (2002).
[12]R. N. Rohling, A. H. Gee, and L. Berman, "Automatic registration of 3-D ultrasound images," Ultrasound Med. Biol. **24**, 841–854 (1998).
[13]R. Kohavi, Presented at the IJCAI, 1995.
[14]N. J. A. Sloane and D. W. Aaron, "Prediction and entropy of printed English," in *Claude E. Shannon: Collected Papers* (Wiley-IEEE, NJ, 1993), pp. 194–208.
[15]J. P. Pluim, J. B. Maintz, and M. A. Viergever, "Image registration by maximization of combined mutual information and gradient information," IEEE Trans. Med. Imaging **19**, 809–814 (2000).
[16]G. G. Zeng, T. S. McGowan, T. M. Larsen, L. M. Bruce, N. K. Moran, J. R. Tsao, and M. S. MacPherson, "Calcifications are potential surrogates for prostate localization in image-guided radiotherapy," Int. J. Radiat. Oncol., Biol., Phys. **72**, 963–966 (2008).
[17]C. Hoffmann, S. Krause, E. M. Stoiber, A. Mohr, S. Rieken, O. Schramm, J. Debus, F. Sterzing, R. Bendl, and K. Giske, "Accuracy quantification of a deformable image registration tool applied in a clinical setting," J. Appl. Clin. Med. Phys. **15**, 237–245 (2014).
[18]B. J. Davis, E. M. Horwitz, W. R. Lee, J. M. Crook, R. G. Stock, G. S. Merrick, W. M. Butler, P. D. Grimm, N. N. Stone, L. Potters, A. L. Zietman, and M. J. Zelefsky, "American Brachytherapy Society consensus guidelines for transrectal ultrasound-guided permanent prostate brachytherapy," Brachytherapy **11**, 6–19 (2012).
[19]P. Orio, K. Wallner, G. Merrick, A. Herstein, P. Mitsuyama, K. Thornton, W. Butler, and S. Sutlief, "Dosimetric parameters as predictive factors for biochemical control in patients with higher risk prostate cancer treated with Pd-103 and supplemental beam radiation," Int. J. Radiat. Oncol., Biol., Phys. **67**, 342–346 (2007).
[20]M. A. Papagikos, A. F. Deguzman, P. J. Rossi, D. L. McCullough, P. E. Clark, and W. R. Lee, "Dosimetric quantifiers for low-dose-rate prostate brachytherapy: Is V(100) superior to D(90)?," Brachytherapy **4**, 252–258 (2005).
[21]W. J. Morris, M. Keyes, D. Palma, M. Mckenzie, I. Spadinger, A. Agranovich, T. Pickles, M. Liu, W. Kwan, J. Wu, V. Lapointe, E. Berthelet, H. Pai, R. Harrison, W. Kwa, J. Bucci, V. Racz, and R. Woods, "Evaluation of dosimetric parameters and disease response after 125 iodine transperineal brachytherapy for low- and intermediate-risk prostate cancer," Int. J. Radiat. Oncol., Biol., Phys. **73**, 1432–1438 (2009).
[22]R. Nath, W. S. Bice, W. M. Butler, Z. Chen, A. S. Meigooni, V. Narayana, M. J. Rivard, and Y. Yu, "AAPM recommendations on dose prescription and reporting methods for permanent interstitial brachytherapy for prostate cancer: Report of Task Group 137," Med. Phys. **36**, 5310–5322 (2009).
[23]W. R. Crum, T. Hartkens, and D. L. G. Hill, "Non-rigid image registration: theory and practice," Br. J. Radiol. **77**, S140–S153 (2004).
[24]M. L. Kessler, "Image registration and data fusion in radiation therapy," Br. J. Radiol. **79**, S99–S108 (2006).
[25]N. Kirby, C. Chuang, U. Ueda, and J. Pouliot, "The need for application-based adaptation of deformable image registration," Med. Phys. **40**, 011702 (10pp.) (2013).
[26]K. K. Brock, "Results of a multi-institution deformable registration accuracy study (MIDRAS)," Int. J. Radiat. Oncol., Biol., Phys. **76**, 583–596 (2009).
[27]V. Narayana, P. L. Roberson, A. T. Pu, H. Sandler, R. H. Winfield, and P. W. McLaughlin, "Impact of differences in ultrasound and computed tomography volumes on treatment planning of permanent prostate implants," Int. J. Radiat. Oncol., Biol., Phys. **37**, 1181–1185 (1997).
[28]R. G. Stock, N. N. Stone, A. Tabert, C. Iannuzzi, and J. K. DeWyngaert, "A dose–response study for I-125 prostate implants," Int. J. Radiat. Oncol., Biol., Phys. **41**, 101–108 (1998).
[29]L. Potters, Y. Cao, E. Calugaru, T. Torre, P. Fearn, and X.-H. Wang, "A comprehensive review of CT-based dosimetry parameters and biochemical control in patients treated with permanent prostate brachytherapy," Int. J. Radiat. Oncol., Biol., Phys. **50**, 605–614 (2001).
[30]M. J. Zelefsky and W. F. Whitmore, Jr., "Long-term results of retropubic permanent 125iodine implantation of the prostate for clinically localized prostatic cancer," J. Urol. **158**, 23–29 (1997).